Bioorganic & Medicinal Chemistry 18 (2010) 2575–2585

Contents lists available at ScienceDirect

Bioorganic & Medicinal Chemistry

journal homepage: www.elsevier.com/locate/bmc

Novel DNA–peptide interaction networks

Jonathan T. B. Huang [a], Yen-Chung Chen [a], Jung-Cheng Chang [a], Kee-Ching G. Jeng [b], Karen K. L. Kao [a], Robin C. K. Yang [a], Lou-Sing Kan [c,d], Ming-Tsair Wey [c], Michael J. Waring [e], Chee-Shan Chen [f], Wei-Jyun Chien [f], Leung Sheh [a,*]

[a] Department of Chemistry and Life Science Research Center, Tunghai Christian University, Taichung 407, Taiwan, ROC
[b] Department of Medical Research, Taichung Veterans General Hospital, Taichung 405, Taiwan, ROC
[c] Institute of Chemistry, Academia Sinica, Taipei 115, Taiwan, ROC
[d] Department of Bioengineering, Tatung University, Taipei 104, Taiwan, ROC
[e] Department of Pharmacology, University of Cambridge, Tennis Court Road, Cambridge CB2 1PD, United Kingdom
[f] Department of Applied Chemistry, Chaoyang University of Technology, Taichung 413, Taiwan, ROC

ARTICLE INFO

Article history:
Received 6 January 2010
Revised 19 February 2010
Accepted 19 February 2010
Available online 2 March 2010

Keywords:
DNA–peptide molecular recognition
Positive cooperative binding
Footprinting
Circular dichroism
Interaction networks

ABSTRACT

Allostery in the binding of peptides to DNA has been studied by quantitative DNase I footprinting using four newly designed peptides containing the XP(Hyp)RK motif and *N*-methylpyrrole (Py) moieties. Apparent binding constants in the micromolar range as well as Hill coefficients were determined for each peptide. The results, together with previous studies on five other peptides support the proposal that interaction network cooperativity is highly preferred in DNA–peptide interactions that involve multiple recognition sites. It is envisaged that interstrand bidentate interactions participate in the relay of conformational changes between recognition sites on the complementary strands. Models for interpreting DNA allostery based upon interaction networks are outlined. Circular dichroism experiments involving the titration of peptides against a short oligonucleotide duplex indicate that some of these peptides bind in a dimeric manner to DNA via the minor groove, inducing characteristic conformational changes. These insights should prompt the design of new DNA-binding peptides for investigating allosteric interactions between peptides and DNA, as well as novel interaction networks, and ultimately may shed light upon the fundamental chemical rules that govern allostery in more complex biological process such as DNA–protein interaction networks.

© 2010 Elsevier Ltd. All rights reserved.

1. Introduction

An understanding of sequence-specific or sequence-selective binding of small molecules to DNA is important for unraveling molecular aspects of the modulation of gene expression. Its fruits lie in the progress of much structural biochemistry research as well as drug design.[1–3] To this end extensive studies have been carried out on synthetic conjugates containing 4-amino-1-methylpyrrole-2-carboxylic acid residues (Py) which are related to the antiviral antibiotics netropsin and distamycin.[4–10]

Early in the study of DNA sequence-specific agents we introduced a novel XPRK[11] tetrapeptide motif which is a modification of the naturally-occurring SPXX motif[12,13] found in repeating sequences in histones, steroid hormone receptors, various segmentation gene products and some oncogene products. It was suggested that the SPXX motif assumes a β-turn stabilized by two hydrogen bonds, and that the side chains of the two basic residues engage in salt bridges with the DNA phosphate groups. Further conjugation of two XPRK motifs with Py residues yielded peptides having high affinity for DNA sequences.[14] We showed that peptides designed in this manner bind preferentially to DNA at sites containing consecutive A's or T's and often engage in interstrand bidentate interactions[14,15] with the bases of DNA (two or more hydrogen bonds formed between a hydrogen donor of an amino acid residue and a base pair in the minor groove). Because peptides incorporating XPRK motifs have binding constants in the micromolar or submicromolar range they fulfill an essential requirement for affording satisfactory DNA footprints.[11,14,16,17,20]

Allostery is recognized as a central process in biological control governing biochemical efficiency and energy expenditure, having been investigated for more than half a century. However, much less is known about allosteric features of DNA–ligand interactions than protein–ligand interactions.[21] In studies on the sequence-selective behavior of many synthetic peptides containing both the XP(Hyp)RK motif and the polyamide motif, we identified a number that show significant positive cooperativity in binding to adjacent recognition sites on the DNA duplex. Among these ligands a newly-synthesized dodecapeptide His-Hyp-Arg-Lys-(Py)$_4$-Lys-Arg-Hyp-His-NH$_2$ (**RHyp-12**) has been investigated in detail.

* Corresponding author. Tel.: +886 4 23590248; fax: +886 4 23590426.
E-mail address: Lsheh@thu.edu.tw (L. Sheh).

0968-0896/$ - see front matter © 2010 Elsevier Ltd. All rights reserved.
doi:10.1016/j.bmc.2010.02.047

Peptide RHyp-12 is a derivative of a parent compound His-Pro-Arg-Lys-$(Py)_4$-His-Pro-Arg-Lys-NH_2 (**PyPro-12**; formerly named **PyH-12**) in which the proline of PyPro-12 is replaced by a hydroxyproline residue, furnishing an extra hydroxyl group for additional hydrogen bonding. Another peptide His-Pro-Arg-Lys-$(Py)_4$-Lys-Arg-NH_2 (**PyHK-10**) contains only one X-Pro-Arg-Lys motif, and was designed as a C-terminal truncated derivative of the parent peptide PyPro-12. Similarly, truncation of the C-terminal dipeptide fragment Hyp-His affords the decapeptide His-Hyp-Arg-Lys-$(Py)_4$-Lys-Arg-NH_2 (**HyH-10**). Further truncating the penultimate lysyl residue of peptide PyHK-10 affords the nonapeptide His-Pro-Arg-Lys-$(Py)_4$-Arg-NH_2 (**PyHR-9**).

For the past decade, it has been recognized that network-based interactions between bio-molecules exist in many biochemical and physiological processes in nature.[18,19] High-throughput interaction studies have also established protein–protein interaction networks, metabolic networks, and transcription regulatory networks.[18] In 2006 we proposed a network-based DNA–peptide allosteric interaction model interconnecting multiple DNA sites in fragments of the latent membrane protein (LMP-1) gene from a pathogenic Epstein-Barr virus variant derived from nasopharyngeal carcinoma.[17] Recently we proposed three different types of network-based allosteric communication between synthetic peptides binding to DNA: circuit type, incomplete-circuit type, and non-circuit type characterized by interstrand bidentate interactions.[20] In the present study we set out to explore the structural basis for molecular recognition and cooperativity in allosteric DNA interaction networks using the four designed peptides described above, employing quantitative DNase I footprinting as the major methodology. In addition, to investigate molecular aspects of the processes we resorted to circular dichroism experiments which provide an invaluable spectral probe of DNA–peptide interactions.

2. Results and discussion

Quantitative footprinting, using a 5′-^{32}P-labeled 158-mer DNA duplex and a complementary 5′-^{32}P-labeled 135-mer DNA duplex,[14] was employed as the major methodology for this study since most other methods fail to discriminate multiple binding sites on the DNA double helix (binding sites are designated U and L referring to the upper and lower strands, respectively). Monodentate interactions and interstrand bidentate interactions between peptide moieties and the DNA bases have been recognized as an essential basis of DNA–protein[15] and DNA-small ligand[14,20] sequence-specific or sequence-selective recognition. The positions of interstrand bidentate interactions can be assigned by connecting bases (with pecked lines)

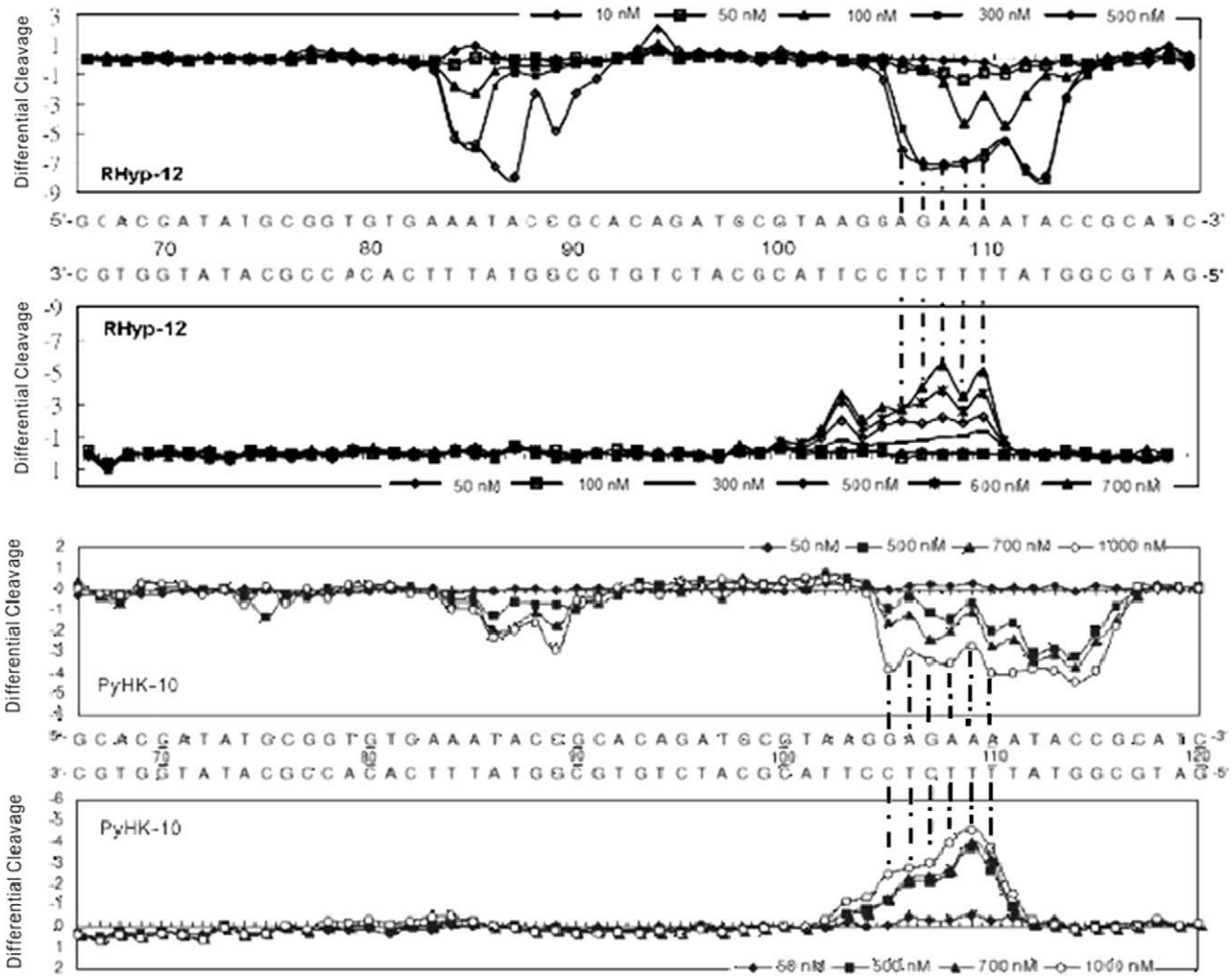

Figure 1. Differential cleavage plots comparing the susceptibility of DNA fragments to DNase I cleavage after incubation with each peptide in cacodylate buffer at room temperature for 60 min. The upper traces represent the differential cleavage plot for a given peptide bound to the 5′-[^{32}P]-labeled upper strand (158-mer) DNA fragment; the lower traces represent the corresponding plots for each peptide bound to the 5′-[^{32}P]-labeled lower strand (135-mer) DNA fragment. The vertical dotted lines between DNA bases represent assignment of interstrand bidentate interactions where significant coincident H-bonding interactions occur between complementary bases in both strands.

where significant simultaneous DNase I blockages on the complementary strands appear in differential cleavage plots (Fig. 1).

On the upper strand of the 158-mer fragment, binding of peptide RHyp-12 produces two major DNase I blockage sites: position U106–113, corresponding to the sequence 5′-AGAAAATA-3′ (Figs. 1 and 2A) and displaying significant positive cooperativity (n_H = 2.1); and position U84–90, comprising the sequence 5′-AATACCG-3′ also showing positive cooperativity (n_H = 1.5). On the lower strand, peptide RHyp-12 elicits a wide DNase I blockage site at position L110–103 corresponding to the sequence 5′-TTTCTCCT-3′, again showing positive cooperativity (n_H = 2.0). From the differential cleavage plots, five interstrand bidentate interactions can be assigned at position 106–110, comprising the self-complementary sequence 5′-AGAAA-TTTCT-3′ (Fig. 1, Table 1).

On the 158-mer upper strand, the decapeptide PyHK-10 produces strong and broad DNase I blockage extending from position U105 to 115, corresponding to the sequence 5′-GAGAAAATACC-3′ and displaying significant positive cooperativity (n_H = 2.4) (Figs. 1 and 2B). At a peptide concentration of 1000 nM, a region of weak and broad DNase I blockage is also observed around position U86–89, corresponding to the sequence 5′-TACC-3′ and displaying weak negative cooperativity. On the 135-mer lower strand, peptide PyHK-10 shows a single DNase I blockage site around position L111–105, corresponding to the sequence 5′-TTTTCTC-3′ and displaying only weak positive cooperativity (n_H = 1.4). Three interstrand bidentate interactions are assigned around position 105–111. Unlike peptide RHyp-12 and the parent peptide PyPro-12,[20] peptide PyHK-10 does not seem to exhibit any preference for

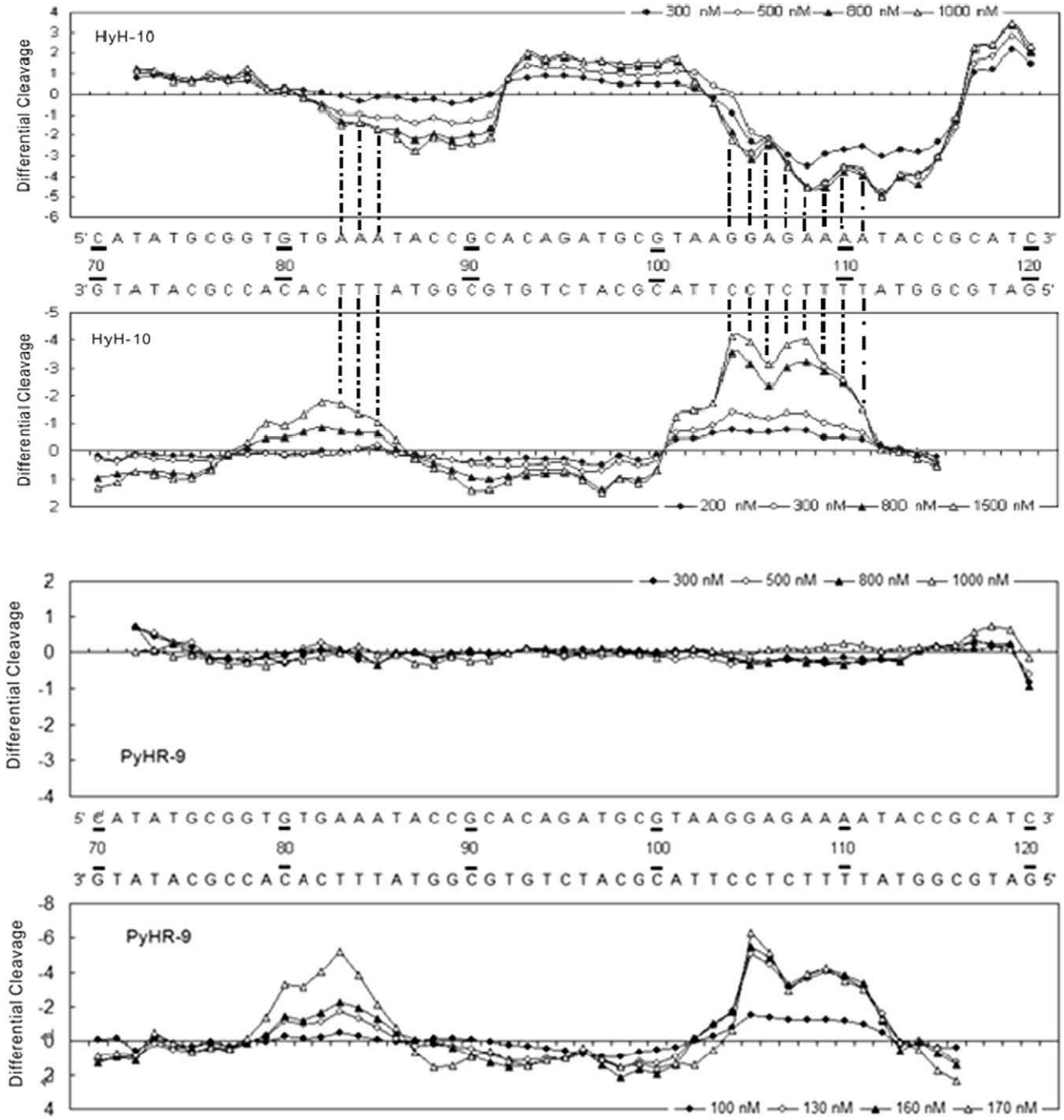

Fig. 1 (*continued*)

binding to two of the three consecutive A residues on the upper strand around position U83–85 but it does in binding to position U86–89 comprising the sequence 5′-TACC-3′ (Figs. 1 and 2B). This discrepancy in DNA sequence preference at the same binding site manifested by PyHK-10 compared to peptides RHyp-12 and Py-Pro-12 can be attributed to the truncated structure of PyHK-10.

The sequence preference of decapeptide HyH-10 (Figs. 1 and 2C) is quite different from that of peptides RHyp-12 and PyHK-10. On the upper strand peptide HyH-10 induces strong and very broad DNase I blockage around position U104–115, corresponding to the sequence 5′-GGAGAAAATACC-3′, displaying positive cooperativity (n_H = 1.7), and there is also a broad DNase I blockage site around position U83–91, comprising the sequence 5′-AAA-TACCGC-3′, where notable positive cooperativity (n_H = 2.6) is evident. On the lower strand, two regions of DNase I blockage appear around positions L85–82, and L111–104. Interstrand bidentate interactions are assigned around positions 83–85 and 104–111 (Fig. 1, Table 1).

Furthermore, the nonapeptide PyHR-9 displays very different DNA sequence preferences from all other peptides studied to date (Fig. i, Supplementary data). At concentrations up to 3000 nM (above which value non-specific peptide binding is evident), no DNase I blockage can be observed on the 158-mer upper strand. Peptide PyHR-9 appears to have a rather strong binding site on the lower strand, where saturation is observed around a peptide concentration of 190 nM (Fig. i, Supplementary data). Two DNase I blockages can be seen around position L85–79, corresponding to the sequence 5′-TTTCACA-3′, displaying high positive cooperativity (n_H = 5.0), and around position L112–104, comprising the sequence 5′-ATTTTCTCC-3′, where unusually high positive cooperativity (n_H = 10.6) is measured. Comparing peptide PyHR-9 with peptide PyHK-10, the only primary structural difference is that the latter peptide bears an additional lysyl residue at the penultimate C-terminal position. As mentioned above, peptide PyHR-9 refuses to bind to the upper strand, and does not engage in interstrand bidentate interactions (Fig. 1). By contrast, peptide

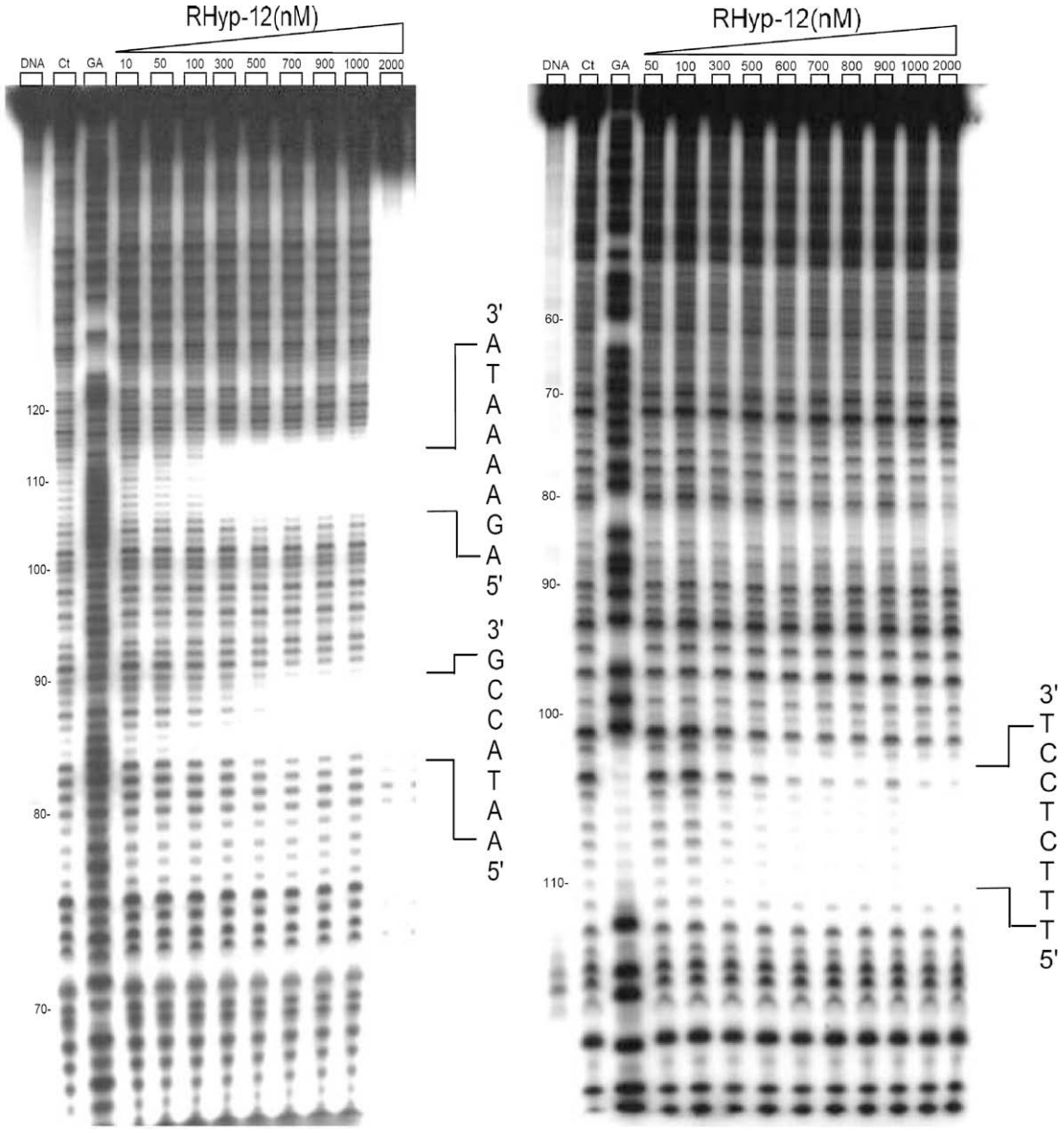

Figure 2A. Autoradiograph showing DNase I footprinting of peptide RHyp-12 on DNA duplexes labeled at the 5′ end: 5′-[^{32}P]-labeled 158-mer upper strand, left panel; and 5′-[^{32}P]-labeled 135-mer lower strand, right panel. Peptide RHyp-12 was equilibrated with the DNA in 5 mM sodium cacodylate buffer, pH 6.5 at 37 °C for 60 min before DNase 1 cleavage. G represents a Maxam–Gilbert guanine sequencing track and Ct shows a DNase I digestion control lane.

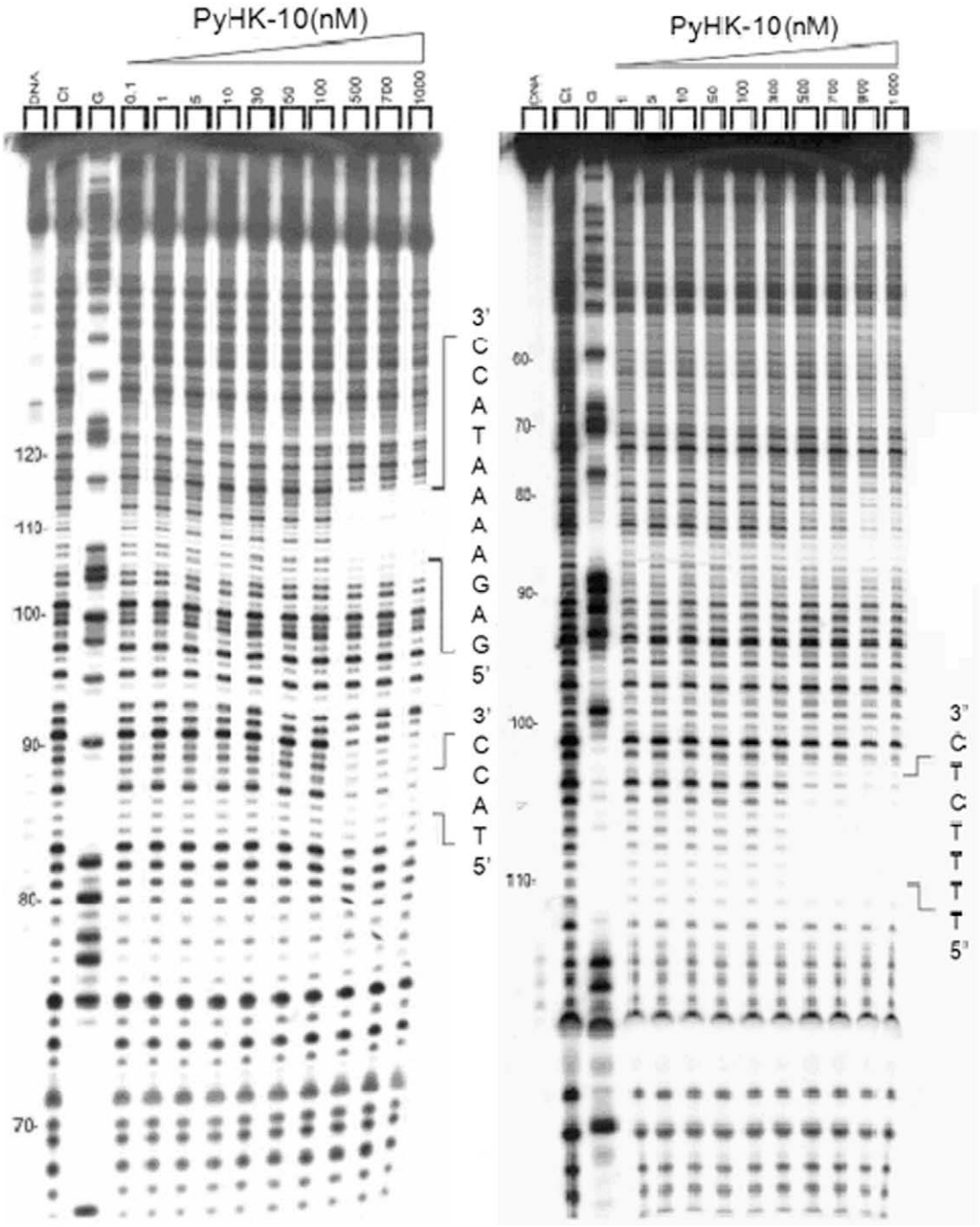

Figure 2B. Autoradiograph showing DNase I footprinting of peptide PyHK-10 on DNA duplexes labeled with [^{32}P] on the 5′ end: 5′-[^{32}P]-labeled 158-mer upper strand, left panel; and 5′-[^{32}P]-labeled 135-mer lower strand, right panel.

PyHK-10 binds strongly to its two major sites on the upper strand and shows interstrand bidentate interactions (Fig. 1). This suggests that at least two Lys or Arg residues near the C-terminal position of the peptide are required for binding to the upper strand binding sites: d(AAAA)- and d(AAA)-. The reason why peptide PyHR-9 appears to engage in unusually strong positive cooperative binding to two sites on the lower DNA strand is unclear and awaits further investigation. However, in a previous investigation,[17] peptides HR-12 and SP-12 that do not manifest interstrand bidentate interactions with LMP-1 gene fragments were also found to show notably strong positive cooperative binding. Thus, we speculate that unusually high positive cooperativity in binding to DNA by small molecules might be related to the absence of interstrand bidentate interactions that probably stabilize local DNA conformation and thus are likely to inhibit strong positive cooperative ligand binding between adjacent sites. The apparent binding constant K_a of the four peptides for the four major binding sites on the pBR322 DNA fragments lie within the range 1.4×10^6–$9.7 \times 10^6\ M^{-1}$. Peptide PyHR-9 gives rise to the two highest apparent binding constants on the 5′-TTTCACA-3′ and 5′-ATTTTCTCC-3′ sites of the lower strand (Table 1).

Based on the footprinting results, we now propose models to interpret the complex communication between DNA–peptide allosteric binding sites for the four designed peptides (Fig. 3). A notable

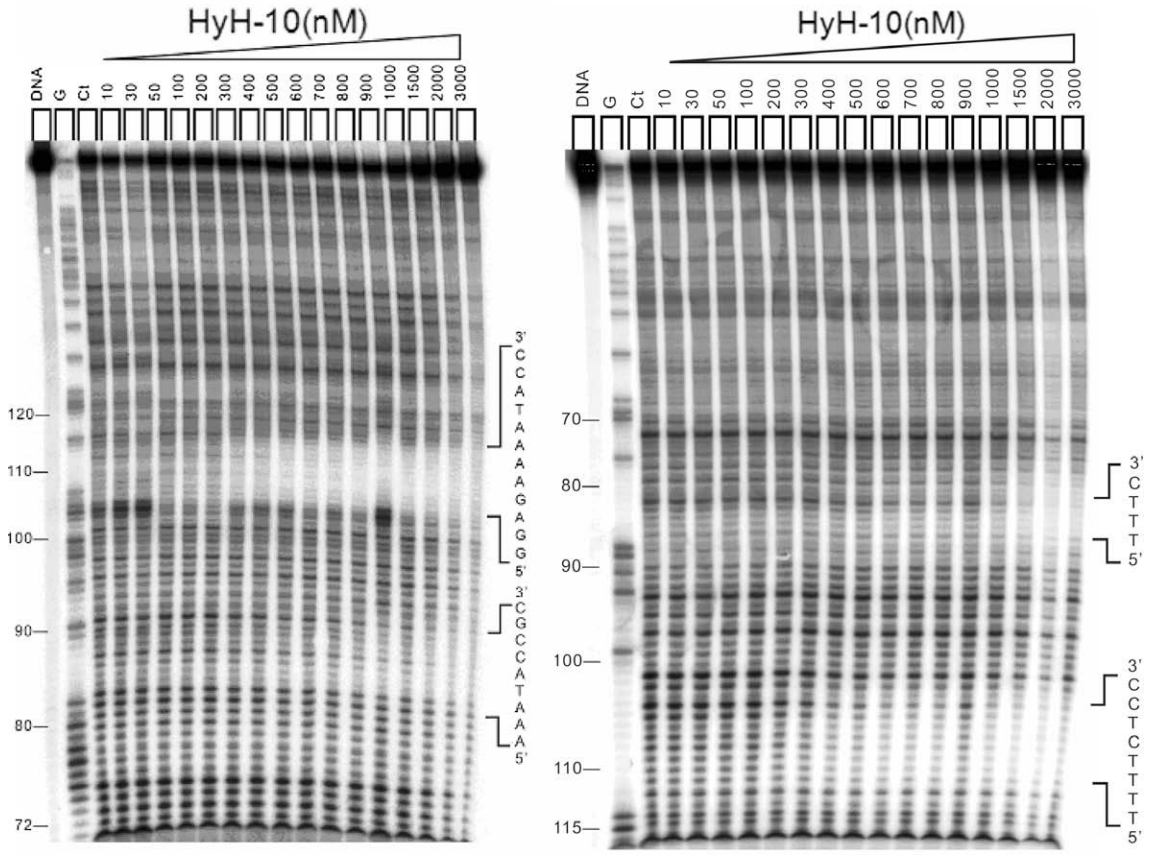

Figure 2C. Autoradiograph showing DNase I footprinting of peptide HyH-10 on DNA duplexes labeled at the 5′ end: 5′-[^{32}P]-labeled 158-mer upper strand, left panel; and 5′-[^{32}P]-labeled 135-mer lower strand, right panel.

Table 1
Binding specificity and physicochemical parameters of sequence-specific binding of peptides to various recognition sites on complementary 5′-[^{32}P]-labeled upper (158-mer) and 5′-[^{32}P]-labeled lower (135-mer) DNA strands at 37 °C determined by quantitative DNase I footprinting

Ligand	Binding site position	Recognition sequence	K_a	n_H	Position of interstrand bidentate interactions
RHyp-12	U84–90	5′-AATACCG-3′	3.0×10^6	1.5	106–110
	U106–113	5′-AGAAAATA-3′	7.6×10^6	2.1	
	L110–103	5′-TTTCTCCT-3′	7.4×10^6	2.0	
PyHK-10	U86–89	5′-TACC-3′	4.9×10^6	0.8	105–110
	U105–115	5′-GAGAAAATACC-3′	2.7×10^6	2.4	
	L111–105	5′-TTTTCTC-3′	3.4×10^6	1.4	
HyH-10	U83–91	5′-AAATACCGC-3′	1.8×10^6	2.6	83–85
	U104–115	5′-GGAGAAAATACC-3′	4.7×10^6	1.7	104–111
	L85–82	5′-TTTC-3′	1.4×10^6	1.3	
	L111–104	5′-TTTTCTCC-3′	3.6×10^6	2.0	
PyHR-9	L85–79	5′-TTTCACA-3′	8.4×10^6	5.0	NIL
	L112–104	5′-ATTTTCTCC-3′	9.7×10^6	10.6	

K_a and n_H are the apparent association constant and Hill coefficient determined from concentration-dependent DNase I footprinting studies, respectively. The binding site positions on the upper and lower strands are abbreviated as U and L, respectively. Interstrand bidentate interactions are assigned where there are coincident effects on

feature is that these models reveal networks of interaction. Put another way, our models point to network-based allosteric connections between recognition sites. Conformational changes occurring at particular binding loci are transmitted to adjacent sub-binding sites and also to sites on the complementary strand, most likely via interstrand bidentate interactions. Allosteric communication may also occur between more remote binding sites, spanning distances up to 12–16 base pairs. Recent footprinting experiments[20] on the 81-mer duplex (S-81) containing a single d(AAAA)–d(TTTT) sequence have shown that the n_H values for peptides PyHyp-12 and PyHyp-9 binding to 81-mer duplexes containing a single binding locus are significantly higher than those for the 158-mer and 135-mer duplexes containing both binding loci. These results suggest that the allosteric relay of peptide binding information to neighboring sites between the d(AAA)–d(TTT) and d(AAAA)–d(TTTT) positions spanning an intervening sequence of 12–14 base pairs may be affected by some negative cooperative effect(s).

It is also notable that the binding of peptides HyH-10 and Py-Pro-12[20] to pBR322 fragments possessing multiple sites reveals what we term a circuit type of allosteric communication within a

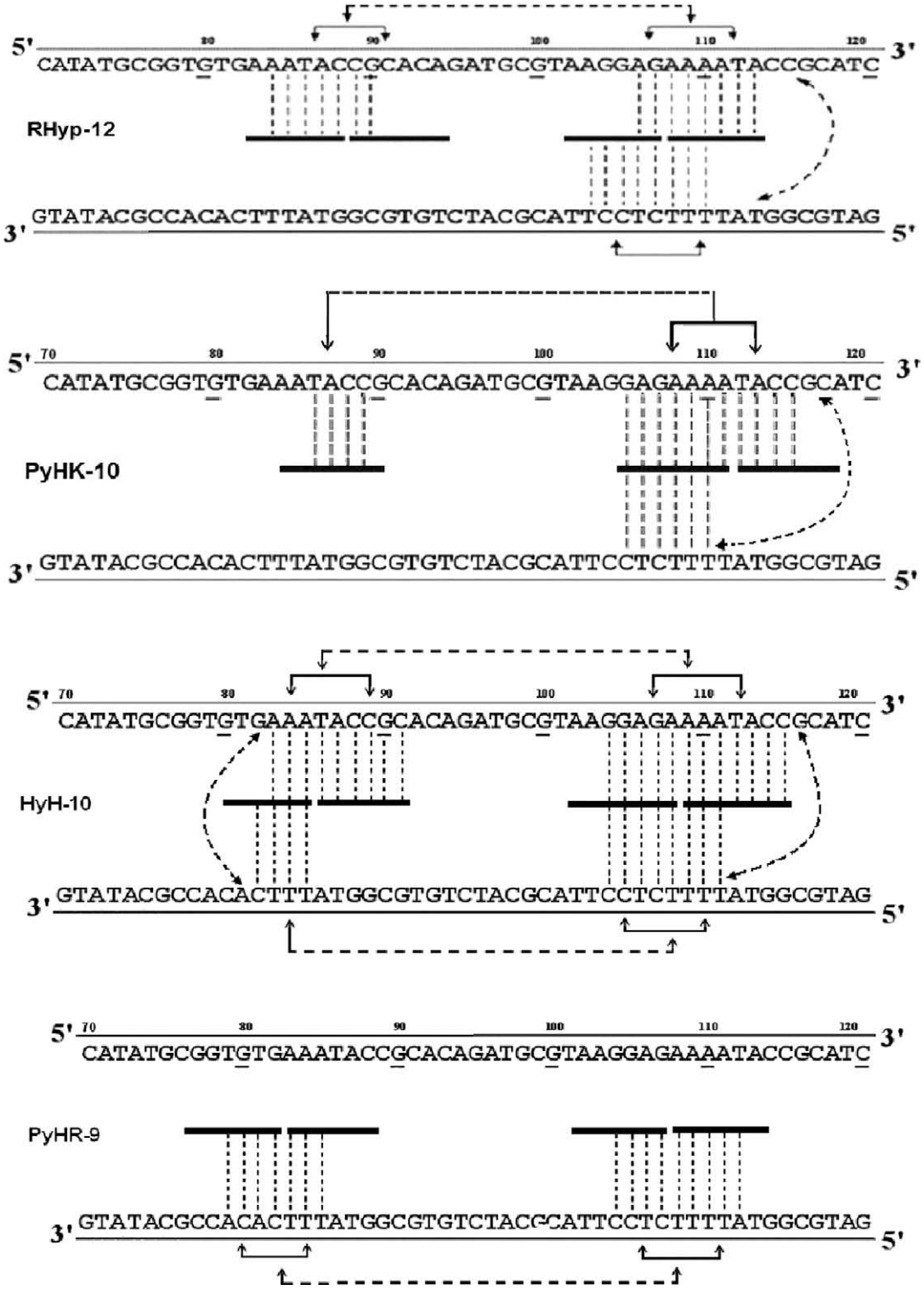

Figure 3. Proposed allosteric models for cooperative binding of peptides RHyp-12, PyHK-10, HyH-10, and PyHR-9 to 158-mer and 135-mer pBR322 fragments based on quantitative footprinting studies. The portion of the ligand binding to each DNA site/sub-site is represented by a thick horizontal line. Monodentate interactions and interstrand bidentate interactions are represented by vertical broken lines. The solid horizontal arrow lines represent communication of allosteric interaction between DNA sub-binding sites. Broken horizontal arrow lines between neighboring binding loci some 12–16 nucleotides apart are intended to represent moderate or weak cooperative communication.

network-based system; that is, the allosteric interactions between binding sites form a closed circuit. For peptides RHyp-12 and PyHK-10, the networks are referred to as incomplete-circuit type; that is, the allosteric communications form a partial or incomplete circuit. On the other hand, peptides PyHR-9, $(HPRK)_3NH_2$ [HR-12],[17] $(SPRK)_3NH_2$ [SP-12][17] whose binding to DNA fragments lacks interstrand bidentate interactions appear to engage in a non-circuit type of allosteric communication.[20]

Thus, the quantitative footprinting results in this work and those reported previously[17,20] support our hypothesis[20] that three

different types of network-based allosteric communication in peptide–DNA molecular recognition can be distinguished: circuit type, incomplete-circuit type and non-circuit type.

To gain insight into conformational changes of DNA associated with the sequence-selective binding of peptides, we carried out circular dichroism studies using the four peptides RHyp-12, PyHK-10, HyH-10 and PyHR-9. A 13-mer deoxyribonucleotide duplex d(TAGGAGAAAATAC)–d(GTATTTTCTCCTA) (U4A-L4T), containing a sequence of 12 base pairs that correspond to the binding site at position 103–114 of the pBR322 fragments was used as substrate. The CD spectra for the DNA and peptides only are shown in Figure 4A.

Titration of peptide RHyp-12 versus the U4A-L4T duplex produces a dose-dependent negative CD enhancement band around 247 nm together with two strong positive CD enhancement bands around 282 nm and 328 nm (Fig. 4B). In the difference spectra the negative band around 247 nm can be seen to be red-shifted to 269 nm and two strong positive bands are seen around 289 nm and 327 nm (Fig. 4C). A near-isoelliptic point occurs at 280 nm, suggesting a two-component binding process. It has been reported in a number of articles[22,23] that molecules which bind to the minor groove typically exhibit an induced positive CD band around 320 nm. Thus, it is safe to conclude that the strong positive CD enhancement bands around 327 nm seen with peptide RHyp-12 and other peptides simply represent binding to the minor groove.

On the other hand, titration of peptide PyHK-10 against the duplex U4A-L4T produces a negative CD band around 248 nm and a positive band around 284 nm (Fig. 4D). The positive CD band extends as a strong and broad dose-dependent positive CD enhancement band up to 332 nm. In the difference spectrum (Fig. 4E) this strong, broad, dose-dependent positive band is shifted to 329 nm whereas the induced positive CD band around 284 nm is shifted to 289 nm. These bands are mostly peptide concentration-dependent, except that the CD band induced by 0.5 μM peptide concentration is blue-shifted while the CD band induced by the highest concentration (5.0 μM) has lowered CD intensity centering around 325 nm. We repeated the CD experiments using 0.5 μM and 5.0 μM peptide concentrations and identical results were obtained. The unusual deviation in ellipticity change of peptide PyHK-10 could be due to an abrupt change in DNA conformation occurring at high peptide concentration (5.0 μM).

The CD spectra seen with peptide HyH-10 are quite similar to those of peptide PyHK-10. Titration of peptide HyH-10 versus the duplex U4A-L4T induces a negative CD band around 247 nm and a positive band around 284 nm (Fig. 4F). A strong, broad, dose-dependent positive CD enhancement appears around 330 nm. In the difference spectrum (Fig. 4G), this CD band around 330 nm is unchanged. Another induced positive CD band is red-shifted from 284 nm to 288 nm.

The CD spectra measured with the nonapeptide PyHR-9 are rather different from those of the decapeptides. Titration of peptide PyHR-9 against the duplex U4A-L4T induces a negative CD band around 249 nm and a positive band around 270 nm (Fig. 4H). A

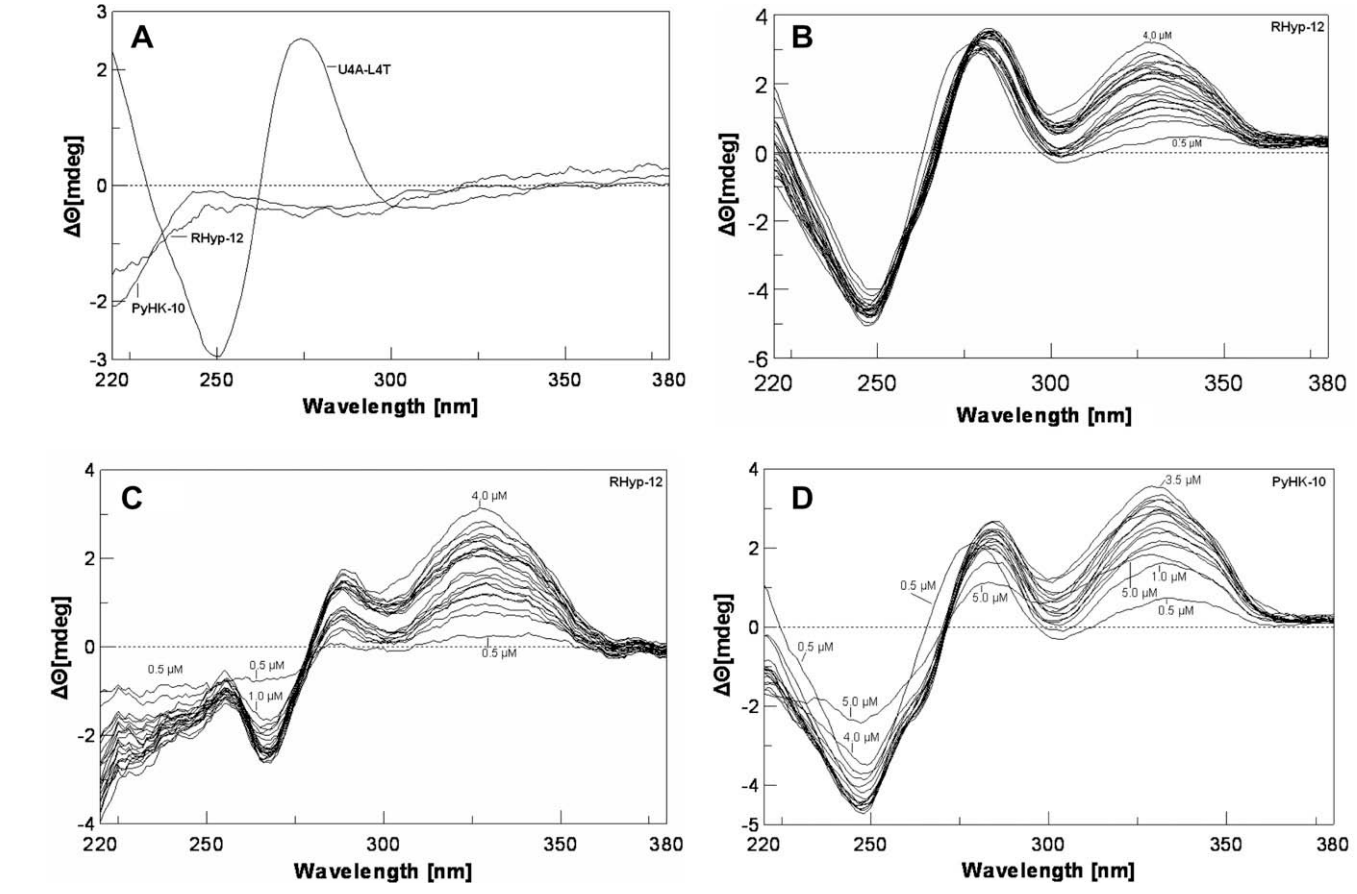

Figure 4. Panel A: CD spectra of DNA duplex U4A-L4T alone and peptide alone. Panel B: Titration of duplex U4A-L4T versus peptide RHyp-12 at peptide concentrations of 0.2, 1.0. 2.2, 2.4, 2.6, 2.8, 3.0, 3.2, 3.4, 4.0, 5.0 μM. Panel C: Corresponding CD difference spectra with the contribution of duplex and peptide RHyp-12 subtracted. Panel D: Titration of duplex U4A-L4T versus peptide PyHK-10 at the same peptide concentrations. Panel E: Corresponding CD difference spectra with the contribution of duplex and peptide PyHK-10 subtracted. Panel F: Titration of duplex U4A-L4T versus peptide HyH-10 at the same peptide concentrations. Panel G: Corresponding CD difference spectra with the contribution of duplex and peptide HyH-10 subtracted. Panel H: Titration of duplex U4A-L4T versus peptide PyHR-9 at the same peptide concentrations. Panel K: Corresponding CD difference spectra with the contribution of duplex and peptide PyHR-9 subtracted.

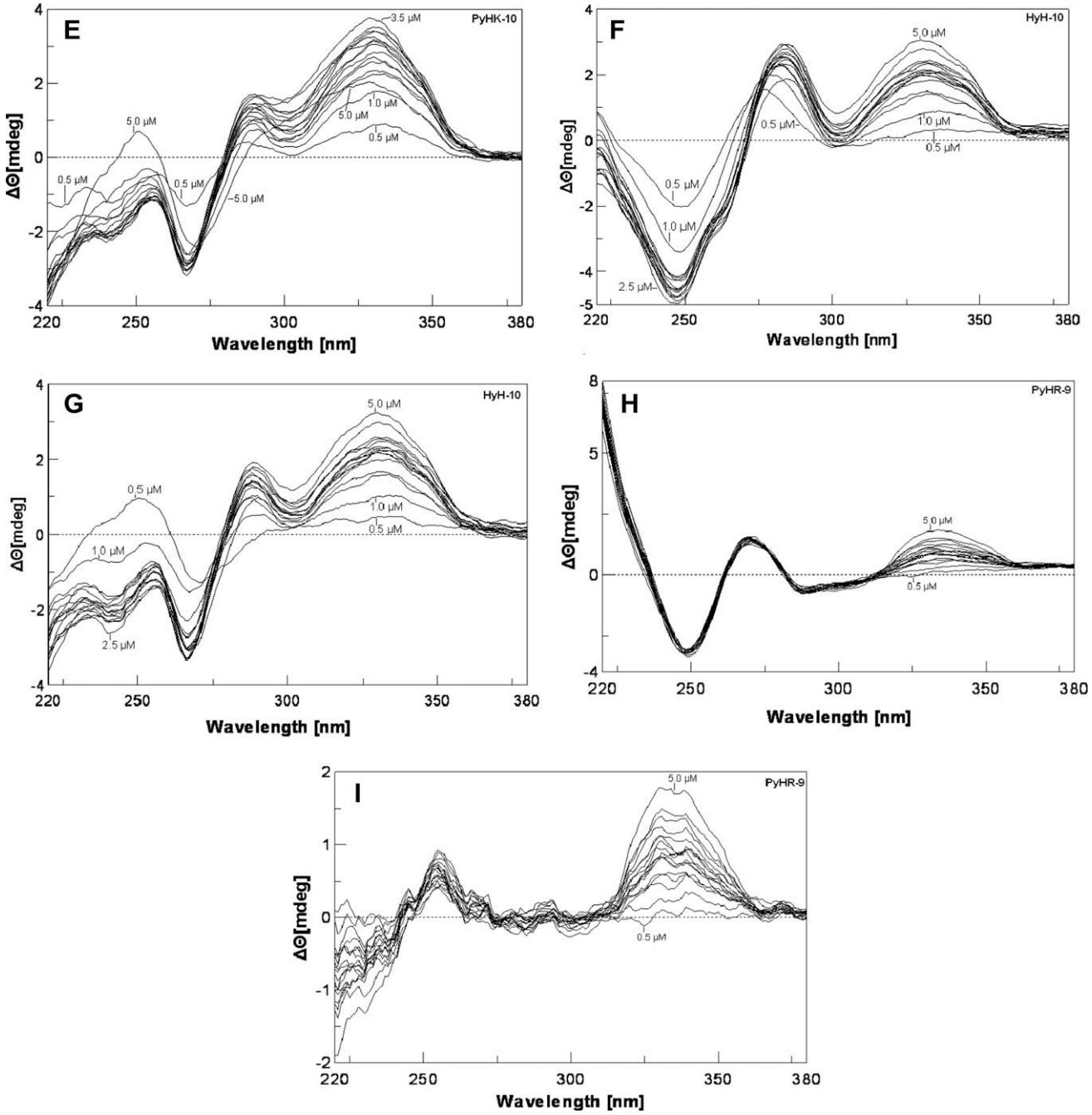

Fig. 4 (*continued*)

wide and shallow positive band is induced around 334 nm. In the difference spectra a weak band occurs around 255 nm and the positive band around 334 nm is unchanged (Fig. 4I).

It is apparent that the peptide-induced enhancement of CD bands is correlated with peptide–DNA binding stoichiometry. Figure 5 shows a plot of [peptide]/[DNA duplex] versus $\Delta\theta$ at 322 nm for peptides RHyp-12, PyHK-10, HyH-10 and PyHR-9. It is evident that the decapeptide PyHK-10 induces the greatest ellipticity change among the four peptides, suggesting that more drastic DNA conformational changes are associated with the binding of this peptide in the minor groove. On the other hand, significantly greater ellipticity changes are induced by peptides PyHK-10, RHyp-12 and HyH-10 compared to nonapeptide PyHR-9, suggesting that much stronger conformational changes are induced in the minor groove by all three former peptides. The ellipticity changes induced by peptides RHyp-12 and HyH-10 are of comparable magnitude.

From the [peptide]/[DNA duplex] plot (Fig. 5), it is apparent that at peptide/DNA ratios of 0.5–2.0, one molecule of peptide binds to the d(AAAA)–d(TTTT) locus. At [peptide]/[DNA duplex] ratios of 2.0–3.0, as indicated by the small plateau region of the titration curve, two peptide molecules seem to bind in a dimeric pattern to the binding site in the minor groove. At [peptide]/[duplex] ratios above 4.0, a progressive increase in $\Delta\theta$ suggests that more peptide molecules begin to engage in some sort of non-sequence-selective binding to DNA. The CD results agree well with other DNase I footprinting results that dimeric peptide binding to the d(AAAA)–d(TTTT) locus is favored, as shown by the very wide binding locus spanning a distance of 9–12 base pairs (Fig. 1, Table 1).

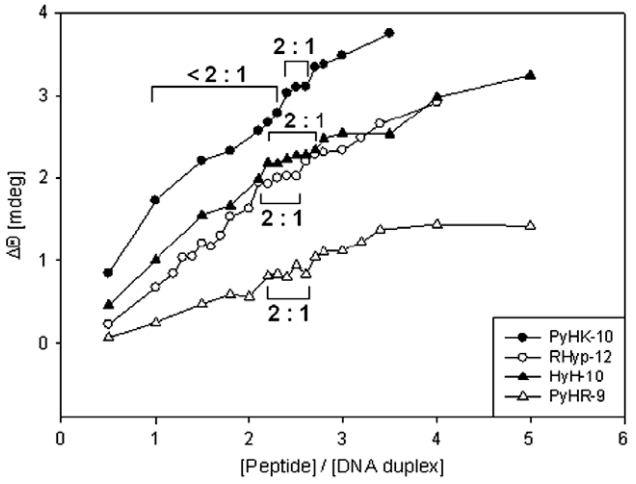

Figure 5. CD intensity at 322 nm as a function of [peptide]/[DNA duplex] The proposed stoichiometric binding ratios are as indicated, with binding below 2:1 (<2:1) considered to be predominantly 1:1.

3. Conclusion

The present study of four peptides, combined with previous studies of five other peptides[17,20] composed of XP(Hyp)RK motifs, supports the proposal that network interaction cooperativity is highly preferred in DNA–peptide interactions that involve multiple recognition sites. It is envisaged that interstrand bidentate interactions participate importantly in the relay of conformational changes between recognition sites on the complementary strands. The present and previous studies[17,20] also lend support to our recent proposal[20] that three different types of allosteric interaction networks can be distinguished in peptide–DNA molecular recognition. Thus, the present work should prompt the design of new DNA-binding peptides for further investigation of DNA–peptide allosteric interactions and DNA interaction networks. In addition, by extending the footprinting approach for studying DNA allosteric interaction networks to multiple DNA-small molecule interactions we may gain useful insights into the fundamental chemical rules that govern allostery in more complex biological process such as DNA–protein interaction networks.

4. Experimental

4.1. Chemicals and biochemicals

All the protected amino acid derivatives were purchased from Bachem California (Torrance, CA) and AnaSpec, Inc. (San Jose, CA). All peptides are synthesized in our laboratory. All other analytical reagents were purchased from Acros, Tedia or Sigma. The radiolabeled nucleoside triphosphate [γ-^{32}P]ATP was obtained from NEN Life Science Products at a specific activity of 6000 Ci/mmol. *Taq* polymerase, T4 polynucleotide kinase, and DNase I were purchased from Promega. All other chemicals were analytical grade reagents, and all solutions were prepared using deionized, Millipore-filtered water.

4.2. Solid-phase peptide synthesis

4.2.1. His-Pro-Arg-Lys-(Py)$_4$-Lys-Arg-NH$_2$ (PyHK-10)

This peptide was synthesized using solid phase methodology by manual operation of a Protein Technology PS3 peptide synthesizer. The first Fmoc-protected amino acid was coupled to the Nova Rink amide AM resin using PyBOP/NMM in DMF. All of the N$_\alpha$-Fmoc-protected amino acids (in 4 equiv ratio excess to the resin) were coupled in a stepwise fashion using PyBOP/NMM in DMF after deprotection of the N$_\alpha$-Fmoc group by piperidine. The side chains of Arg, Lys, Tyr and His are protected by the Pmc, Boc and Trt groups, respectively. After coupling the last N-terminal Fmoc-amino acid residue, the resin was treated with the cleavage reagent (0.75 g phenol, 10 mL TFA, 0.5 mL thioanisole, 0.25 mL EDT) for 1.5 h, and then lyophilized. The resin was washed with dry ether (2 × 30 mL), filtered, and then washed with 5% acetic acid (200 mL). The combined filtrate was lyophilized and the product was purified by semi-preparative reversed-phase HPLC (column 1) using gradient elution. Eluent A: 5% MeCN, 95% H_2O, 0.1% TFA; Eluent B, 95% MeCN, 5% H_2O, 0.1% TFA. A linear gradient was achieved by increasing the MeCN content from eluent A to eluent B in 30 min t_R (column 2), 11.93 min, mp 144–146 °C, $[\alpha]_D^{24}$ −46.78 (*c* 0.043, MeOH/H_2O, 1:1); ESIMS requires: 1308.5, found: 1309.0.

4.2.2. His-Hyp-Arg-Lys-(Py)$_4$-Lys-Arg-Hyp-His-NH$_2$ (RHyp-12)

This peptide was synthesized and purified to homogeneity using a similar procedure as for peptide PyHK-10. t_R (column 2), 11.65 min mp 159–162 °C, $[\alpha]_D^{24}$ −14.28 (*c* 0.035, MeOH/H_2O, 1:1); ESIMS requires: 1574.75, found: 1574.93.

4.2.3. His-Hyp-Arg-Lys-(Py)$_4$-Lys-Arg-NH$_2$ (HyH-10)

This peptide was synthesized and purified to homogeneity using a similar procedure as for peptide PyHK-10. t_R (column 2), 14.63 min, mp 153–157 °C, $[\alpha]_D^{27}$ −14.0 (*c*, 0.262 MeOH/H_2O, 1:1); ESIMS requires: 1324.50, found: 1325.18.

4.2.4. His-Pro-Arg-Lys-(Py)$_4$-Arg-NH$_2$ (PyHR-9)

This peptide was synthesized and purified to homogeneity using a similar procedure as for peptide PyHK-10. t_R (column 2), 15.29 min, mp 150–153 °C, $[\alpha]_D^{27}$ −28.33 (*c*, 0.20 MeOH/H_2O, 1:1); ESIMS requires: 1180.53, found: 1180.38.

4.3. Polymerase chain reaction (PCR) and end-labeling of PCR products

The 5′-^{32}P-labeled 158-mer DNA duplex and 5′-^{32}P-labeled 135-mer DNA duplex were prepared by PCR amplification in a thermal cycler (ABI model 9700) as reported previously.[14] The DNA concentration was determined by UV spectroscopy to lie in the range 600–800 nM.

4.4. DNase I footprinting

Reactions were conducted in a total volume of 10 μL. Radiolabeled DNA (2 μL) was mixed with varying concentrations of peptide (2 μL) dissolved in 5 mM sodium cacodylate buffer, pH 6.5 and equilibrated at room temperature for 120 min. DNase I (2 μL) was added and the reaction allowed to proceed at 37 °C for 10 min. The DNase I solution (in 20 mM NaCl, 2 mM $MgCl_2$, 2 mM $CaCl_2$) was adjusted to yield a final concentration of 0.009 unit/mL so as to limit the digestion to less than 30% of the starting material in order to minimize the incidence of multiple cleavages in any one strand. The digestion was stopped by adding stop solution (4 μL) containing 80% formamide, 10 mM EDTA, 0.1% bromophenol blue, and 0.1% xylene cyanol. Samples were heated at 90 °C for 4 min and chilled on ice for 4 min prior to electrophoresis. The products of DNase I cleavage were resolved by polyacrylamide gel electrophoresis under denaturing conditions (0.3 mm thick, 8% acrylamide containing 8 M urea). After electrophoresis (about 1.45 h at 70 Watts, 1800 V in TBE buffer, BRL sequencer model S2), gels were soaked in 10% acetic acid/10% methanol for 15 min, transferred to Whatman 3MM paper, dried under vacuum at 80 °C for 45 min. The autoradiographs (footprinting of peptides

RHyp-12 and PyHK-10) were obtained by using Kodak BioMax MR scientific imaging films with intensifying screens for about 5 days. The autoradiographs (footprinting of peptides HyH-10 and PyHR-9) were obtained by placing the dried gels against an imaging plate (BAS-MS2340) of a Fuji phosphoImager FLA-5100 overnight. The electrophoretic band areas were analyzed by a PC computer installed with Viber Lourmat BIO-ID software (Marne La Valle, Cedex 1, France).

The apparent DNA binding site saturation is determined by the equation:[9]

$$Y' = 1 - (I_{tot}/I_{ref})/(I^{o}_{tot}/I^{o}_{ref})$$

where Y' is the fractional saturation, I_{ref} and I^{o}_{ref} are integrated band volumes of 5 bases of a running lane (non-binding site, with peptide) and control lane (without peptide), respectively. I_{tot} and I^{o}_{tot} are integrated band volumes of the binding site locus and corresponding control lane locus, respectively.

The value of Y is optimized by the following equation:

$$Y = (Y' - Y'_{min})/(Y'_{max} - Y'_{min})$$

where Y'_{max} and Y'_{min} are the maximum and minimum site saturation Y' values, respectively.

The Hill coefficients were determined by the Hill equation: $\mathrm{Log}[Y/1-Y] = \log K_a + n_H \log[L]$ where Y is the fractional saturation, [L] the peptide concentration, and n_H the Hill coefficient. A minimum of six data points within or near the linear portion of binding isotherm (Y vs Log [L]) were carefully chosen for the Hill plot ($\mathrm{Log}\, Y/(1-Y)$ vs Log [L]) using a linear least-squares fitting procedure by Sigma Plot software (version 8.0). The Hill coefficient was determined from the slope of the corresponding Hill plot. The apparent binding constant K_a is determined empirically as the peptide concentration at 50% fractional saturation from the binding isotherm.

4.5. Circular dichroism (CD) studies

CD spectra were measured at 37 °C with a Jasco J-815 instrument in the Institute of Chemistry, Academia Sinica. The duplex DNA was adjusted to 1.0 μM in 5 mM sodium cacodylate buffer (pH 6.5) and peptides, dissolved in the same buffer, were added to maintain final concentrations of 0.2, 1.0, 2.2, 2.4, 2.6, 2.8, 3.0, 3.2, 3.4, 4.0, 5.0 μM. CD spectra were recorded after 60 min incubation at 37 °C.

Acknowledgments

We thank Miss L.M. Hsu, National Chung-Hsing University for ESI mass analyses. This work was supported by Grant NSC97-2113-M029-005 from the National Science Council, ROC.

Supplementary data

Supplementary data associated with this article can be found, in the online version, at doi:10.1016/j.bmc.2010.02.047.

References and notes

1. Waring, M. J.. In *Antibiotics*; Hahn, F. E., Ed.; Springer: Berlin, 1979; Vol. 5, pp 173–194.
2. Moravek, Z.; Neidle, S.; Schneider, B. *Nucleic Acids Res.* **2002**, *30*, 1182–1191.
3. Fox, K. R.; Waring, M. J. *Methods Enzymol.* **2001**, *340*, 412–430.
4. Hudson, J. S.; Brooks, S. C.; Graves, D. E. *Biochemistry* **2009**, *48*, 4440–4447.
5. Chen, Y. H.; Lown, J. W. *J. Am. Chem. Soc.* **1994**, *116*, 6995–7005.
6. Bailly, C.; Suh, D.; Waring, M. J.; Chaires, J. B. *Biochemistry* **1998**, *37*, 1033–1045.
7. Walker, W. L.; Landaw, E. M.; Dickerson, R. E.; Goodsell, D. S. *Proc. Natl. Acad. Sci. U.S.A.* **1997**, *94*, 5634–5639.
8. Chen, F. M.; Sha, F.; Chin, K. H.; Chou, S. H. *Nucleic Acids Res.* **2004**, *32*, 271–277.
9. Mrksich, M.; Parks, M. E.; Dervan, P. B. *J. Am. Chem. Soc.* **1994**, *116*, 7983–7988.
10. Fechter, E. J.; Dervan, P. B. *J. Am. Chem. Soc.* **2003**, *125*, 8476–8485. and references cited therein.
11. Yang, C. H.; Chou, P. J.; Luo, Z. L.; Chang, J. C.; Cheng, C. C.; Martin, C. R. H.; Waring, M. J.; Sheh, L. *Bioorg. Med. Chem.* **2003**, *11*, 3279–3288.
12. Churchill, M. E. A.; Suzuki, M. *EMBO J.* **1989**, *8*, 4189–4195.
13. Suzuki, M. *Nature* **1990**, *344*, 562–565.
14. Chang, J. C.; Yang, C. H.; Chou, P. J.; Yang, W. H.; Chou, I. C.; Lu, C. T.; Lin, P. H.; Hou, R. C. W.; Jeng, K. C. G.; Cheng, C. C.; Sheh, L. *Bioorg. Med. Chem.* **2004**, *12*, 53–61.
15. Luscombe, N. M.; Laskowski, R. A.; Thornton, J. M. *Nucleic Acids Res.* **2001**, *29*, 2860–2869.
16. Yang, C. H.; Chen, W. F.; Jong, M. C.; Jong, B. J.; Chang, J. C.; Waring, M. J.; Ma, L.; Sheh, L. *J. Am. Chem. Soc.* **2004**, *126*, 8104–8105.
17. Yang, C. H.; Jeng, K. C. G.; Yang, W. H.; Chen, Y. L.; Hung, C. C.; Lin, J. W.; Chen, S. T.; Richardson, S.; Martin, C. R. H.; Waring, M. J.; Sheh, L. *ChemBioChem* **2006**, *7*, 1187–1196.
18. Russell, R. B.; Aloy, P. *Nat. Chem. Biol.* **2008**, *4*, 666–673.
19. Palla, G.; Derenyi, E.; Farkas, T.; Vicsek, T. *Nature* **2005**, *435*, 814–818.
20. Kao, K. L.; Jonathan, C. T.; Huang, J. C. T.; Yang, C. K.; Jeng, K. C. G.; Chang, J. C. C.; Yao, W. C.; Hsien, S. C.; Waring, M. J.; Chen, M. H.; Ma, L.; Sheh, L. *Bioorg. Med. Chem.* **2010**, *18*, 366–376.
21. Koshland, D. E., Jr.; Hamadani, K. *J. Biol. Chem.* **2002**, *277*, 46841–46844. and references cited therein.
22. Buchmueller, K. L.; Staples, A. M.; Howard, C. M.; Horick, S. M.; Uthe, P. B.; Le Minh, N.; Cox, K. K.; Nguyen, B.; Pacheco, K. A. O.; Wilson, W. D.; Lee, M. *J. Am. Chem. Soc.* **2005**, *127*, 742–750.
23. Munde, M.; Lee, M.; Neidle, S.; Arafa, R.; Boykin, D. W.; Liu, Y.; Bailly, C.; Wilson, W. D. *J. Am. Chem. Soc.* **2007**, *129*, 5688–5698.